crystals

MDPI

Article

Indium-Incorporation with $In_xGa_{1-x}N$ Layers on GaN-Microdisks by Plasma-Assisted Molecular Beam Epitaxy

ChengDa Tsai [1], Ikai Lo [1,*], YingChieh Wang [1], ChenChi Yang [1], HongYi Yang [1], HueiJyun Shih [1], HuiChun Huang [1], Mitch M. C. Chou [1], Louie Huang [2] and Binson Tseng [2]

[1] Department of Physics, Department of Materials and Optoelectronic Science, Center for Nanoscience and Nanotechnology, National Sun Yat-Sen University, Kaohsiung 80424, Taiwan; d002030010@student.nsysu.edu.tw (C.T.); d982030006@student.nsysu.edu.tw (Y.W.); d002030005@student.nsysu.edu.tw (C.Y.); d042030008@student.nsysu.edu.tw (H.Y.); shepherd3319@gmail.com (H.S.); m9036601@student.nsysu.edu.tw (H.H.); mitch@faculty.nsysu.edu.tw (M.M.C.C.)

[2] Advanced Semiconductor Engineering, Inc., Kaohsiung 811, Taiwan; louie_huang@aseglobal.com (L.H.); Binson_Tseng@aseglobal.com (B.T.)

* Correspondence: ikailo@mail.phys.nsysu.edu.tw

Received: 9 May 2019; Accepted: 12 June 2019; Published: 14 June 2019

Abstract: Indium-incorporation with $In_xGa_{1-x}N$ layers on GaN-microdisks has been systematically studied against growth parameters by plasma-assisted molecular beam epitaxy. The indium content (x) of $In_xGa_{1-x}N$ layer increased to 44.2% with an In/(In + Ga) flux ratio of up to 0.6 for a growth temperature of 620 °C, and quickly dropped with a flux ratio of 0.8. At a fixed In/(In + Ga) flux ratio of 0.6, we found that the indium content decreased as the growth temperature increased from 600 °C to 720 °C and dropped to zero at 780 °C. By adjusting the growth parameters, we demonstrated an appropriate $In_xGa_{1-x}N$ layer as a buffer to grow high-indium-content $In_xGa_{1-x}N$/GaN microdisk quantum wells for micro-LED applications.

Keywords: plasma-assisted molecular beam epitaxy; InGaN; GaN-microdisks

1. Introduction

III-nitride compounds have been extensively studied for applications in optoelectronics [1,2] and spintronics [3,4]. Recently, the GaN-based micro light-emitting diodes (LEDs) have attracted worldwide attention as energy-sustainable lighting sources and for use in full-color displays due to their compact size, high efficiency, and reliability. [5,6] However, micro-LEDs based on InGaN/GaN quantum wells (QWs) are limited by the poor quality of high-indium-content $In_xGa_{1-x}N$/GaN QWs (i.e., $x > 0.33$; so-called green gap) for use in red-green-blue (RGB) full-color displays [7]. Alternatively, some researchers have combined UV InGaN/GaN LED arrays with CdSe/ZnS nanocrystal quantum dots (QDs) for color conversion [8,9] or specialized nano-ring light-emitting diodes (NRLEDs) produced using nano-sphere lithography technology. [10,11] These methods struggled with either introducing foreign CdSe/ZnS QDs or using a nano-lithography for manufacturing. The method of nano-lithography involved reducing the volume of LEDs by an etching process, which resulted in damage to the LED sidewall. Therefore, if one can fabricate micro-LEDs using a single material system, i.e., $In_xGa_{1-x}N$/GaN QWs on self-assembled micro-metered GaN disks, the manufacturing of RGB micro-LED display will become more efficient by a simple process without any complicated nano-lithography. The bandgap energy of ternary compound $In_xGa_{1-x}N$ can be tuned according to the indium content (x) from 0.7 eV (i.e., InN for $x = 1$) to 3.4 eV (i.e., GaN for $x = 0$). In other words, full-color RGB micro-LED displays

can be achieved by the single material system $In_xGa_{1-x}N$/GaN QW with various indium contents (e.g., x ~ 0.13 for blue, x ~ 0.28 for green, and x ~ 0.45 for red). [12–14] However, as the indium volatilized temperature is about 650 °C, it is difficult to grow the $In_xGa_{1-x}N$ layer with a high indium content by high-temperature growths like vapor phase epitaxy or metalorganic chemical vapor deposition. [15] Currently, M. Azadmand et al. studied a droplet-controlled growth dynamics of InGaN/GaN on Si(111) substrate by plasma-assisted molecular beam epitaxy (PAMBE) at low temperatures (e.g., 450 °C), in which the Si(111) substrate provided a hexagonal basis for the growth of ***c***-plane (0001) wurtzite GaN film. [16] In contrast, Lo et al. developed a low-temperature growth of hexagonal ***c***-plane wurtzite GaN microdisks on $LiAlO_2$ (LAO) substrates by PAMBE, where the LAO substrate provided a hexagonal basis for the growth of ***c***-plane $(000\bar{1})$ GaN and meanwhile offered a rectangular basis for *M*-plane $(1\bar{1}00)$ GaN growth. [17] It was shown that 3-dimensional (3D) hexagonal ***c***-plane GaN $(000\bar{1})$ microdisk was grown atop the hexagonal oxygen sites of LAO substrate as a finite GaN microdisk was formed. [18] The 3D GaN microdisk can be used as a "nearly" free-standing GaN substrate for the further growth of $In_xGa_{1-x}N$/GaN, as shown in Figure 1a. However, the lattice constant between GaN (***a*** = 0.3160 nm, ***c*** = 0.5125 nm) and InN (***a*** = 0.3545 nm, ***c*** = 0.5703 nm) is quite different, the fabrication of ternary $In_xGa_{1-x}N$ alloy on the 3D GaN microdisk is crucial for the $In_xGa_{1-x}N$/GaN micro-LED manufacturing. The nucleation of Ga or In atoms is the first step in the formation of $In_xGa_{1-x}N$ layers for self-assembling on N-face, which depends on the thermodynamic chemical potentials of Ga and In ions at equilibrium, $\mu_{Ga}(T)$ and $\mu_{In}(T)$, as shown in Figure 1b. After the nucleation, the In-content (x) of ternary $In_xGa_{1-x}N$ alloy will be affected by the flux ratios between Ga and In molecular beams. The ball-stick model of the ternary $In_xGa_{1-x}N$ alloy starting to grow onto N-face layer of GaN microdisk is simulated with different indium contents, as shown in Figure 1c–f; here, we do not include the lattice deformation due to strain. Therefore, the self-assembling mechanism for different indium contents can be controlled by growth parameters (e.g., substrate temperature and element flux ratio). In this paper, we will systematically study the growth mechanism for the alloy composition of $In_xGa_{1-x}N$ layer on GaN microdisk as functions of growth temperature and flux ratio using low-temperature PAMBE. Based on the results, we demonstrate the growth of high-indium-content $In_xGa_{1-x}N$/GaN quantum well on GaN microdisk for RGB micro-LED applications.

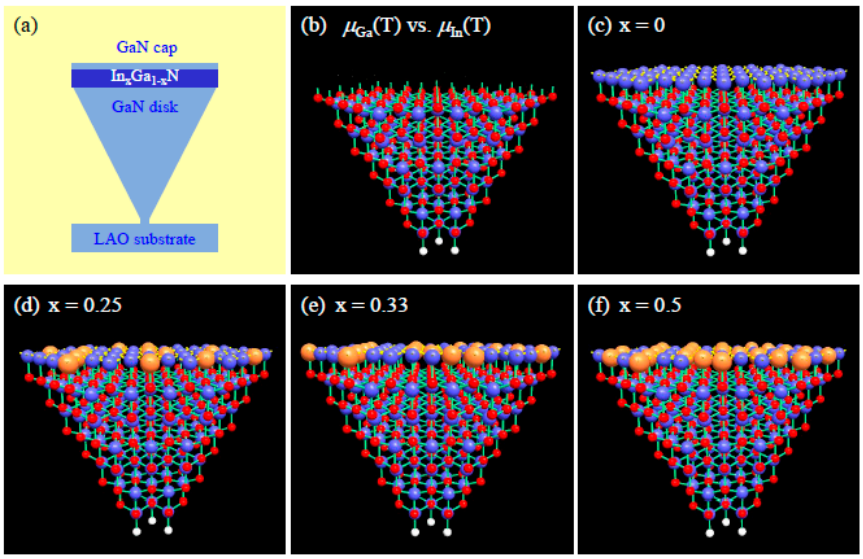

Figure 1. (**a**) The schematic diagram of $In_xGa_{1-x}N$ layer and GaN cap layer on GaN microdisk. (**b**) The ball-stick model for N-face GaN microdisk. (**c**–**f**) The ball-stick models of the ternary $In_xGa_{1-x}N$ layer on N-face layer of GaN microdisk with different indium contents (x = 0, x = 0.25, x = 0.33, and x = 0.5). The slight deformation from the lattice position due to different atomic size will produce some structural defects after stacked fault or dislocation.

2. Materials and Methods

The ternary $In_xGa_{1-x}N$ epi-layers were grown on GaN microdisks on 1 x 1 cm^2 LAO substrates by PAMBE (Veeco Applied-GEN 930 (Hsinchu, Taiwan)) with standard effusion cells for Ga- and In-evaporation and an rf-plasma cell with 450 W for N_2-plasma source. The detailed procedure can be found in our previous papers [17,18]. Before mounting on a holder, the LAO substrates were cleaned with acetone (5 min), isopropanol (5 min), de-ionized water (5 sec), phosphoric acid (1:30) (5 min), de-ionized water (5 sec), and then dried by nitrogen gas, sequentially. After the cleaning, the LAO substrates were out-gassed in MBE chamber at 680 °C for 10 min. Thereafter, the substrate temperature was decreased to the growth temperatures (T_S) specified for the study. The Ga wetting layer was first deposited on the LAO substrate for 5 min at 630 °C, and then a two-step method (i.e., two different N/Ga flux ratios, 29.0 and 138.8, performed for 35 min and 70 min, respectively) was used to grow 3D GaN microdisks at 630 °C. After the GaN epi-layer, we grew $In_xGa_{1-x}N$ epi-layers on the 3D GaN microdisks for different growth parameters designed in Tables 1 and 2. In sample series I, the $In_xGa_{1-x}N$ epi-layers of five samples (samples A–E) were grown at a fixed N flux ratio (BEP = 9.0 x 10^{-6} torr) but the different In/(In + Ga) flux ratios for 90 min at 620 °C, as shown in Table 1. The flux ratio was measured by beam equivalent pressure (BEP) reading from Veeco Applied-GEN 930 system. In sample series II, another four samples with different $In_xGa_{1-x}N$ epilayers were grown at different temperatures but using the same flux ratio as sample D for 90 min for comparison, labelled as samples F, G. H. and I. The detail growth parameters for sample series II are shown in Table 2.

Table 1. The growth parameters for sample series I as a function of flux ratio at N flux BEP = 9.0 × 10^{-6} torr.

Sample Name	In/(In+Ga) Ratio	Growth Temp. (°C)
Sample A	0.2	620
Sample B	0.4	620
Sample C	0.5	620
Sample D	0.6	620
Sample E	0.8	620

Table 2. The growth parameters for sample series II as a function of growth temperature.

Sample Name	In/(In+Ga) Ratio	Growth Temp. (°C)
Sample F	0.6	600
Sample D	0.6	620
Sample G	0.6	640
Sample H	0.6	720
Sample I	0.6	780

In order to examine the microstructure of the samples, two typical InGaN/GaN microdisk specimens were selected from samples D and H for scanning electron microscope (SEM), transmission electron microscope (TEM) and selective area electron diffraction (SAD) measurements. The TEM specimen was prepared by a dual-beam focus ion beam (FIB) along [$1\bar{1}00$] direction, as shown in the Figure 2(a1). The cross-sectional TEM image of 2.49 μm microdisk for sample D is shown in Figure 2(a2). We performed the selection area diffraction (SAD) measurements on the $In_xGa_{1-x}N$ layers at the spot circled in Figure 2(a2). The SAD pattern exhibited a clear wurtzite single crystal as shown in Figure 2(a3). The $In_xGa_{1-x}N$ epi-layers were precisely evaluated by high-resolution TEM images focused on the spots HR1 and HR2, shown in Figure 2(a4,a5). Figure 2(a4) shows the ***c***-plane wurtzite InGaN and Figure 2(a5) shows the interface between GaN and $In_xGa_{1-x}N$ in sample D. The lattice deformation due to the different atomic size can be clearly observed from the $In_xGa_{1-x}N$ epi-layers in Figure 2(a5). Similarly, the TEM specimen of sample H was prepared, Figure 2(b1). The cross-sectional TEM image of the 2.57 μm microdisk is shown in Figure 2(b2). We performed the SAD measurements

on the $In_xGa_{1-x}N$ layer at the spot circled in Figure 2(b2). The SAD pattern exhibited a clear wurtzite crystal as shown in Figure 2(b3). The $In_xGa_{1-x}N$ epi-layers were evaluated by high-resolution TEM images on the spots HR1 and HR2, shown in Figure 2(b4,b5). Figure 2(b4) shows the well-established ***c***-plane wurtzite InGaN and Figure 2(b5) shows the interfaces between GaN and InGaN layers in sample H. Again, the slight lattice deformation of $In_xGa_{1-x}N$ epi-layers can be observed in Figure 2(b5), due to the different sizes between Ga and In atoms.

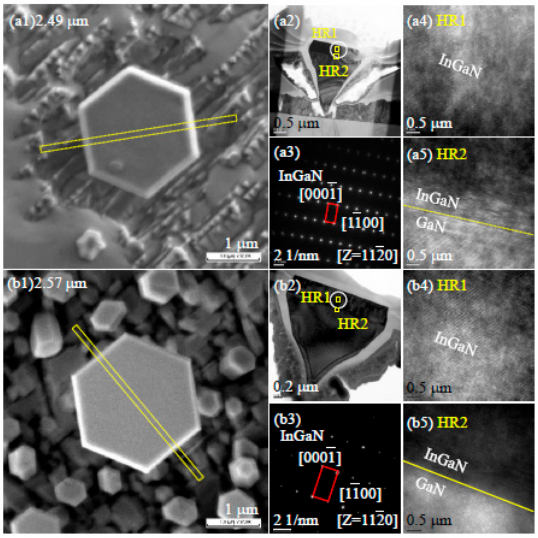

Figure 2. (**a1**) The top view SEM image of the microdisk of Sample D and the cleavage plane along the [1$\bar{1}$00] direction (the scale bar is 1 μm). (**a2**) The TEM image of microdisk (the scalebar is 0.5 μm). (**a3**) The SAD pattern of $In_xGa_{1-x}N$ layer with scale bar of 2 (1/nm). (**a4**,**a5**) show the high-resolution TEM images of the GaN layer, and the interface between GaN layer and $In_xGa_{1-x}N$ layer on microdisk, respectively. (**b1**) The top view SEM image of the microdisk of Sample H and the cleavage plane along the [1$\bar{1}$00] direction (the scalebar is 1 μm). (**b2**) The TEM image of the microdisk (the scale bar is 0.5 μm). (**b3**) The SAD pattern of $In_xGa_{1-x}N$ layer with scale bar of 2 (1/nm). (**b4**,**b5**) show the high-resolution TEM images of the GaN layer, and the interface between GaN layer and $In_xGa_{1-x}N$ layer on microdisk, respectively.

3. Results and Analyses

$In_xGa_{1-x}N$/GaN microdisks of the two series samples were systematically used to evaluate optical properties by cathodoluminescence (CL) and secondary electron images (SEI) measurements (JEOL JSM-6330). Figure 3 shows the results of CL measurement for series I samples. We obtained the CL spectra by detecting the photon energy from 1.8 eV to 3.7 eV at accelerative voltage of 10 kV and extraction voltage of photonelectric magnitude tube of 1.1 kV. In sample A, we observed the highest peak at (2.56 ± 0.003) eV with FWHM equal to (0.088 ± 0.003) eV, the secondary peak at (3.35 ± 0.003) eV with FWHM equal to (0.091 ± 0.007) eV, and the smallest peak at (3.57 ± 0.005) eV with FWHM equal to (0.082 ± 0.003) eV. The SEI and the CL image at the highest peak are shown in Figure 3(a1,a2). The CL image shows that the highest peak for the wavelength of 480 nm (e.g., 2.58 eV) was majorly emitted from the $In_xGa_{1-x}N$ layer itself. The secondary peak (i.e., 3.35 eV) was normally contributed from the GaN layer and the third peak (i.e., 3.57 eV) might be attributed to the microstructures around the InGaN/GaN microdisk. In sample B, we observed the first peak at (2.13 ± 0.005) eV with FWHM equal to (0.137 ± 0.005) eV, the secondary peak at (3.33 ± 0.003) eV with FWHM equal to (0.059 ± 0.004) eV. The SEI and CL images are shown in Figure 3(b1,b2), with the CL image shown at the peak of wavelength 580 nm (e.g., 2.14 eV). In sample C, we observed the first peak at (2.11 ± 0.005) eV with FWHM equal to (0.195 ± 0.008) eV, the secondary peak at (3.38 ± 0.003) eV with FWHM equal to (0.044 ± 0.004) eV. The SEI and CL images are shown in Figure 3(c1,c2). The CL image shows the peak for wavelength of 587 nm (e.g., 2.11 eV). In sample D, we observed the first peak at (2.10 ± 0.009) eV

with FWHM equal to (0.258 ± 0.009) eV, the secondary peak at (3.39 ± 0.005) eV with FWHM equal to (0.045 ± 0.006) eV. The SEI and CL images are shown in Figure 3(d1,d2). The CL image shows the peak for wavelength of 570 nm (e.g., 2.11 eV). In sample E, we observed the first peak at (2.21 ± 0.009) eV with FWHM equal to (0.153 ± 0.003) eV, the secondary peak at (3.37 ± 0.003) eV with FWHM equal to (0.061 ± 0.002) eV. The SEI and CL images are shown in Figure 3(e1,e2). The CL image shows the peak for wavelength of 560 nm (e.g., 2.21 eV). From the spectra in Figure 3, we found that the CL intensity from $In_xGa_{1-x}N$ of sample A was about 52 times that from GaN intensity. The CL intensity of $In_xGa_{1-x}N$ for sample B, sample D, and sample E were about 0.73, 0.32, and 0.32 times those from GaN intensity, respectively, and the CL images of $In_xGa_{1-x}N$ of microdisks had no detectable luminescence, as shown in Figure 3(b2,d2,e2). Because we did not introduce any extrinsic impurity during the epitaxy, the broad CL peak with large FWHM was mostly contributed from the structural defects including dislocations, stacked faults and lattice deformations. The broad secondary peak with large FWHM spectra indicated that the lattice deformation occurred after introducing the indium atoms into $In_xGa_{1-x}N$ layers due to the greater atomic size of indium; e.g., x = 0.33 as shown in Figure 1(d). The CL intensity from $In_xGa_{1-x}N$ in sample C was about 0.72 times that from GaN intensity. Figure 3(c1,c2) show that the position of the illuminating was around the microdisk. The CL peaks, FWHMs, and In contents for the samples of series I are summarized in Table 3.

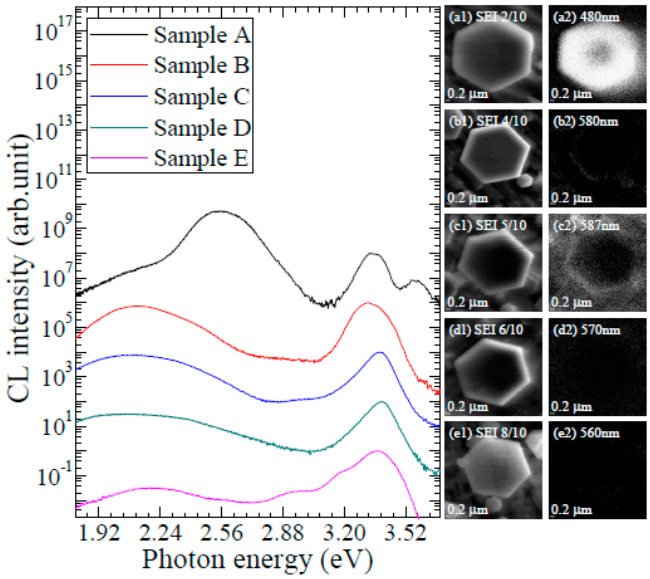

Figure 3. The CL spectra measure at room temperature for samples A to E. (**a1**–**e1**) show the SEI images of Samples A–E and (**a2**–**e2**) show the CL images of the samples for wavelengths of 480 nm,580 nm, 587 nm, 570 nm, and 560 nm, respectively.

Table 3. The summary of CL peak, FWHM, and In content for the samples of series I.

Sample Name	CL Peak of InGaN (eV)	FWHM of CL (eV)	In Content of EDS (%)
Sample A	2.56 ± 0.003	0.088 ± 0.003	17.8 ± 0.92
Sample B	2.13 ± 0.005	0.137 ± 0.005	29.5 ± 0.73
Sample C	2.11 ± 0.005	0.195 ± 0.008	39.3 ± 0.67
Sample D	2.10 ± 0.009	0.258 ± 0.009	44.2 ± 0.83
Sample E	2.21 ± 0.009	0.153 ± 0.003	15.9 ± 4.3

In order to evaluate the constituents of $In_xGa_{1-x}N$ epi-layers, the energy dispersive x-ray spectroscopy (EDS) measurement was performed on the TEM specimens cut from the five series I samples. We prepared the TEM specimens along the $(11\bar{2}0)$ direction and scanning EDS with s zone axis $(10\bar{1}0)$. The result of indium content (x) as a function of In/(In + Ga) flux ratio is shown in Figure 4.

In the insets, Figure 4a–e show the high angle annular dark field (HAADF) TEM images performed in the line EDS scanning mode with the constituent spectra for samples A–E, where the scanning lines were marked on the TEM images. We obtained the EDS constituent spectra (at %) from top surface crossing the $In_xGa_{1-x}N$ layers to the GaN microdisk; Ga content (at %) indicated by black EDS spectrum, In content (at %) by red EDS spectrum and N content (at %) by blue EDS spectrum in the insets. We take an average from the EDS spectra of $In_xGa_{1-x}N$ layers and obtain the indium content of sample A to be (17.8 ± 0.92 %), sample B to be (29.5 ± 0.73 %), sample C to be (39.3 ± 0.67 %), sample D to be (44.2 ± 0.83 %), and sample E to be (15.9 ± 4.3 %). It was found that the content of indium increased when we grew the $In_xGa_{1-x}N$ layer with the In/(In + Ga) flux ratio from 0.2 to 0.6 at the temperature of 620 °C, and dropped quickly when the ratio In/(In + Ga) is up to 0.8. It is shown in the dark field TEM image Figure 4e that the compressive lattice deformation destroyed the shape of wurtzite lattice structure after the incorporation of indium. This is consistent with the worst CL spectrum of sample E shown in Figure 3.

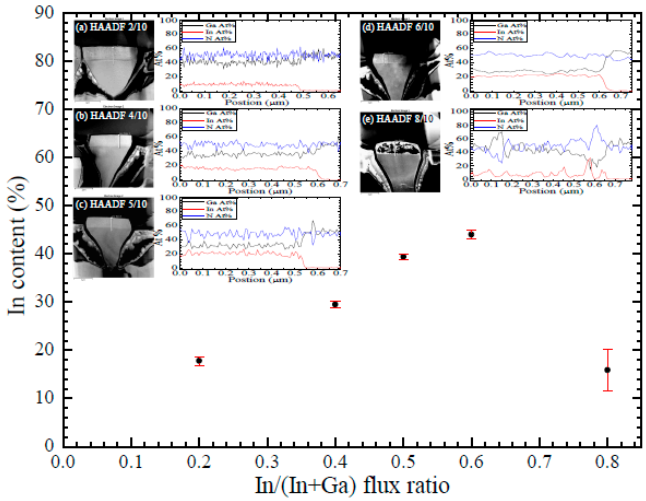

Figure 4. The In contents for sample A to sample E. The insets show the dark field TEM images and the constituent spectra in line scanning mode obtained by EDS, where the scanning lines were marked on the TEM images.

Similar analyses were performed on the series II samples against the growth temperature, where sample D was the same sample as series I for comparison. The results of CL measurements of the series II samples are shown in Figure 5. In sample F, we observed the first peak at (2.21 ± 0.008) eV with FWHM equal to (0.204 ± 0.005) eV, the secondary peak at (2.90 ± 0.005) eV with FWHM equal to (0.083 ± 0.003) eV, and the third peak at (3.37 ± 0.002) eV with FWHM equal to (0.054 ± 0.002) eV. The SEI and CL images are shown in Figure 5(a1,a2), where the CL image shows that the peak for wavelength of 570 nm (e.g., 2.18 eV). For sample D, the CL spectrum is the same as that in Figure 3 for comparison, and the SEI and CL images are shown in Figure 5(b1,b2). In sample G, we observed the first peak at (2.15 ± 0.004) eV with FWHM equal to (0.184 ± 0.004) eV and the secondary peak at (3.36 ± 0.003) eV with FWHM equal to (0.046 ± 0.002) eV. The SEI and CL images are shown in Figure 5(c1,c2). The CL image shows the peak for wavelength of 580 nm (e.g., 2.14 eV). In sample H, we observed the first peak at (2.22 ± 0.004) eV with FWHM equal to (0.098 ± 0.005) eV, the secondary peak at (3.22 ± 0.004) eV with FWHM equal to (0.120 ± 0.006) eV and the third peak at (3.38 ± 0.002) eV with FWHM equal to (0.075 ± 0.003) eV. The SEI and CL images are shown in Figure 5(d1,d2). The CL image shows the peak for wavelength of 580 nm (e.g., 2.14 eV). In sample I, we observed the first peak at (2.25 ± 0.006) eV with FWHM equal to (0.165 ± 0.007) eV and the secondary peak at (3.32 ± 0.002) eV with FWHM equal to (0.057 ± 0.003) eV. The SEI and CL images are shown in the Figure 5(e1,e2). The CL image shows the peak for wavelength of 560 nm (e.g., 2.21 eV). From the CL spectra in Figure 5, we found that the $In_xGa_{1-x}N$ intensity of sample H was about 170 times that of

the GaN intensity. Figure 5(d1,d2) show that the position of the illuminating was from the microdisk. The $In_xGa_{1-x}N$ intensity of sample G was about 40 times that of the GaN intensity. Figure 5(c1,c2) show that the position of the illuminating was around the microdisk. The $In_xGa_{1-x}N$ intensity of sample F was about 0.006 times that of GaN intensity, and the CL image of $In_xGa_{1-x}N$ in microdisk had no detectable luminescence, as shown in Figure 5(a1,a2). The $In_xGa_{1-x}N$ intensity of sample I was about 1.13 times that of GaN intensity. Figure 5(e1,e2) show that the position of the illuminating was around the microdisk edge. The CL peaks, FWHMs, and In contents for the samples of series II are summarized in Table 4.

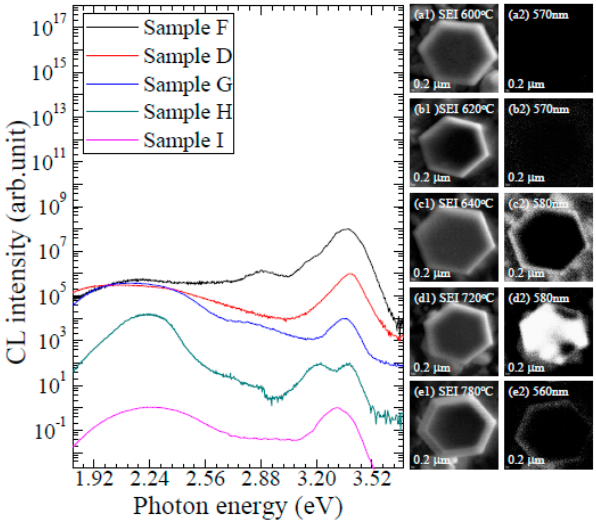

Figure 5. The CL spectra measure at room temperature for samples F, G, H, D, and I. (**a1**–**e1**) show their SEI images. (**a2**–**e2**) show the CL images of the samples for wavelengths of 570 nm,570 nm, 580 nm, 580 nm, and 560 nm, respectively.

Table 4. The summary of CL peaks, FWHMs, and In contents for the samples of series II.

Sample Name	CL Peak of InGaN (eV)	FWHM of CL (eV)	In Content of EDS (%)
Sample F	2.21 ± 0.008	0.204 ± 0.005	53.4 ± 0.75
Sample D	2.10 ± 0.009	0.258 ± 0.009	44.2 ± 0.83
Sample G	2.15 ± 0.004	0.184 ± 0.004	39.8 ± 0.62
Sample H	2.22 ± 0.004	0.098 ± 0.005	34.9 ± 0.72
Sample I	2.25 ± 0.006	0.165 ± 0.007	0%

Again, we evaluate the constituents of $In_xGa_{1-x}N$ layers in series II samples by energy dispersive x-ray spectroscopy (EDS) measurements. The TEM specimens were prepared along the $(11\bar{2}0)$ direction and scanning EDS line mode with the zone axis $(10\bar{1}0)$. The results are shown in Figure 6. The high angle annular dark field (HAADF) TEM images and detailed EDS constituent spectra for series II samples are shown in the insets, Figure 6a–e. The EDS spectra were covered from the top of $In_xGa_{1-x}N$ layer and down to GaN miscrodisk. The indium content of sample F was (53.4 ± 0.75 %), sample D was (44.2 ± 0.83 %), sample G was (39.8 ± 0.62 %), sample H was (34.9 ± 0.72 %), and sample I was (0%). Figure 6 shows that the content of indium decreased with the growth temperature from 600 °C to 720 °C for the epitaxy of $In_xGa_{1-x}N$ layers. When the growth temperature was up to 780 °C, the indium content of $In_xGa_{1-x}N$ layer dropped to zero. This reveals that the high temperature is not favorable for the high-indium-content epitaxy in ternary $In_xGa_{1-x}N$ epi-layers due to the low indium volatilized temperature. Based on the results, we designed an appropriate $In_xGa_{1-x}N$ layer as a buffer to grow high-indium-content $In_xGa_{1-x}N$/GaN microdisk double quantum wells. For instance, after GaN microdisk, we grew the $In_xGa_{1-x}N$ layers as a buffer with flux ratio of (In:Ga:N) to be (9.01×10^{-8} torr: 6.02×10^{-8} torr: 8.96×10^{-6} torr) at temperature of 720 °C for 50 minutes, and capped with a

GaN layer for the further growth of $In_xGa_{1-x}N$/GaN double QWs. The double QWs were grown after the buffer layer with the flux ratio of (In:Ga:N) to be (9.01×10^{-8} torr: 6.02×10^{-8} torr: 8.96×10^{-6} torr) for 1.5 minutes and the flux ratio of (Ga:N) to be (6.02×10^{-8} torr: 9.08×10^{-6} torr) for 30 seconds, and finally the GaN barrier was grown on the GaN cap layer for 5 min with the flux ratio of (Ga:N) to be (1.28×10^{-7} torr: 8.96×10^{-6} torr). This sequence of $In_xGa_{1-x}N$/GaN epi-layers was repeated twice to form $In_xGa_{1-x}N$/GaN double QWs. Figure 7 shows the CL spectrum of the $In_xGa_{1-x}N$/GaN microdisk double QWs, in which the intensity of CL peak at 2.43 eV is about one order of amplitude higher than that at 3.1 eV. The SEM image of the microdisk double QWs is shown in the inset, Figure 7a. The $In_xGa_{1-x}N$ buffer and double-QW structure can be observed from the TEM images, Figure 7b–d. Figure 7e,f show that the CL images of the peak at 2.43 eV, which is mostly emitted from the $In_xGa_{1-x}N$ layers with the In content of x = 0.27 and the CL peak at 3.1 eV which is from microstructures around the microdisk. To confirm the quality of the double QWs, high resolution TEM images were taken at the spots HR01 and HR02, as shown in Figure 7d. The well-assembled GaN lattice and $In_xGa_{1-x}N$ lattice are shown in Figure 7g,h. The slight lattice deformation can only be observed in the $In_xGa_{1-x}N$ layers from high resolution TEM images.

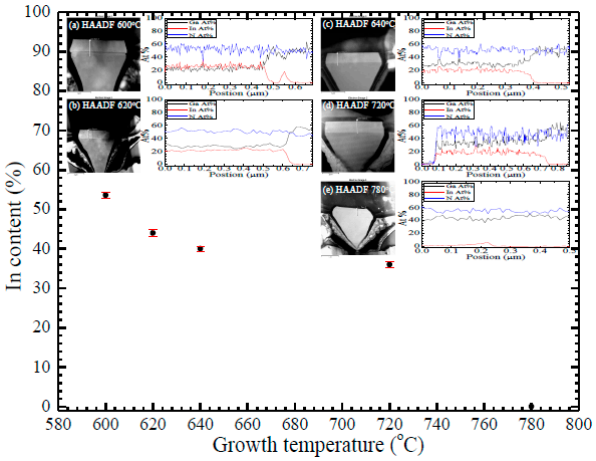

Figure 6. The In contents for sample F, D, G, H, and I. The insets show the dark field TEM images and the constituent spectra in line scanning mode obtained by EDS, where the scanning lines are marked on the TEM images.

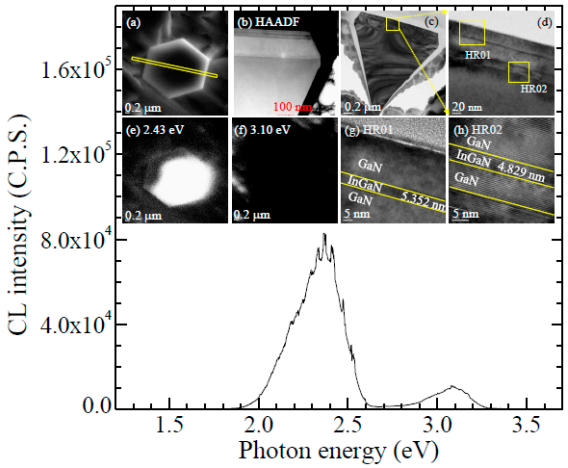

Figure 7. The CL spectrum of the microdisk double QWs. (**a**) The top-view of the microdisk with the cleavage plane along [1$\bar{1}$00] direction (the scale bar is 0.2 μm). (**b**) The high angle annular dark field TEM image. (**c**,**d**) The TEM images for the microdisk double QWs with a scale bar of 0.2 μm and 20 nm. (**e**,**f**) Shows the CL images for photon energies of 2.43 eV, 3.10 eV. (**g**,**h**) Show the high resolution TEM images of the yellow squares in (**d**) which is denoted as HR01 and HR02. The scales bars are 5 nm.

4. Conclusions

We have grown high-indium-content $In_xGa_{1-x}N$ layers on GaN microdisks with a $LiAlO_2$ substrate by low-temperature PAMBE technique. The content (x) of $In_xGa_{1-x}N$ layer increased to 44.2% with the In/(In + Ga) flux ratio up to 0.6 for the growth temperature of 620 °C and quickly dropped with a flux ratio of 0.8. It was shown that the indium-incorporation was limited by the atomic size difference between the III-elements, In and Ga. At a fixed In/(In+Ga) flux ratio, we found that the indium content decreased as the growth temperature increased, revealing that high temperatures are unfavorable for high-indium-content epitaxy in ternary $In_xGa_{1-x}N$ films. Based on these results, we demonstrated that an appropriate $In_xGa_{1-x}N$ layer can be used as a buffer to grow high-quality $In_xGa_{1-x}N$/GaN microdisk quantum wells for micro-LED applications.

Author Contributions: Conceptualization was done by C.T. The experiments were performed and analyzed by C.T., H.Y., H.S., and H.H. The LAO substrate was provisioned by M.M.C.C. Technical assistance provided by Y.W., C.Y., L.H., and B.T., C.T. and I.L. wrote the paper which was revised by all authors.

Acknowledgments: The authors are grateful to Y.-C. Hsu, Y.C. Lin, and H.-C. Hsih for assistance. The project was funded by Ministry of Science and Technology of Taiwan, under the contract 107-2119-M-110-007.

Conflicts of Interest: All of the authors declare no conflict of interest.

References

1. Nakamura, S.; Senoh, M.; Iwasa, N.; Nagahama, S.I.; Yamada, T.; Mukai, T. Superbright Green InGaN Single-Quantum-Well-Structure Light-Emitting Diodes. *Jpn. J. Appl. Phys.* **1995**, *34*, L1332. [CrossRef]
2. Nakamura, S.; Pearton, S.; Fasol, G. *The Blue Laser Diode*, 2nd ed.; Springer: Berlin, Germany, 2000.
3. Lo, I.; Tsai, J.K.; Yao, W.J.; Ho, P.C.; Tu, L.W.; Chang, T.C.; Elhamri, S.; Mitchel, W.C.; Hsieh, K.Y.; Huang, J.H.; et al. Spin splitting in modulation-doped $Al_xGa_{1-x}N$/GaN heterostructures. *Phys. Rev. B* **2002**, *65*, 161306 R. [CrossRef]
4. Lo, I.; Wang, W.T.; Gau, M.H.; Tsai, J.K.; Tsay, S.F.; Chiang, J.C. Gate-controlled spin splitting in GaN/AlNGaN/AlN quantum wells. *Appl. Phys. Lett.* **2006**, *88*, 082108. [CrossRef]
5. Jiang, H.X.; Lin, J.Y. Nitride micro-LEDs and beyond—A decade progress review. *Opt. Express* **2013**, *21*, A475. [CrossRef]
6. Templier, F. GaN-based emissive microdisplays: A very promising technology for compact, ultra-high brightness display systems. *J. Soc. Inf. Disp.* **2016**, *24*, 669. [CrossRef]
7. Auf der Maur, M.; Pecchia, A.; Penazzi, G.; Rodrigues, W.; Di Carlo, A. Efficiency drop in green InGaN/GaN light emitting diodes: The role of random alloy fluctuations. *Phys. Rev. Lett.* **2016**, *116*, 027401. [CrossRef]
8. Chen, K.J.; Chen, H.C.; Tsai, K.A.; Lin, C.C.; Tsai, H.H.; Chien, S.H.; Cheng, B.S.; Hsu, Y.J.; Shih, M.H.; Tsai, C.H.; et al. Resonant-Enhanced Full-Color Emission of Quantum-Dot-Based Display Technology Using a Pulsed Spray Method. *Adv. Funct. Mater.* **2012**, *22*, 5138. [CrossRef]
9. Lee, K.H.; Han, C.Y.; Kang, H.D.; Ko, H.; Lee, C.; Lee, J.; Myoung, N.; Yim, S.Y.; Yang, H. Highly Efficient, Color-Reproducible Full-Color Electroluminescent Devices Based on Red/Green/Blue Quantum Dot-Mixed Multilayer. *ACS Nano* **2015**, *9*, 10941. [CrossRef]
10. Wang, S.W.; Hong, K.B.; Tsai, Y.L.; Teng, C.H.; Tzou, A.J.; Chu, Y.C.; Lee, P.T.; Ku, P.C.; Lin, C.C.; Kuo, H.C. Wavelength tunable InGaN/GaN nano-ring LEDs via nano-sphere lithography. *Sci. Rep.* **2017**, *7*, 42962. [CrossRef]
11. Huang Chen, S.W.; Shen, C.C.; Wu, T.; Liao, Z.Y.; Chen, L.F.; Zhou, J.R.; Lee, C.F.; Lin, C.H.; Lin, C.C.; Sher, C.W.; et al. Full-color monolithic hybrid quantum dot nanoring micro light-emitting diodes with improved efficiency using atomic layer deposition and nonradiative resonant energy transfer. *Photonics Res.* **2019**, *7*, 416. [CrossRef]
12. Schubert, E.F.; Kim, J.K. Solid-State Light Sources Getting Smart. *Science* **2005**, *308*, 1274. [CrossRef] [PubMed]
13. Pimputkar, S.; Speck, J.S.; DenBaars, S.P.; Nakamura, S. Prospects for LED lighting. *Nat. Photonics* **2009**, *3*, 180. [CrossRef]
14. Horiuchi, N. Light-emitting diodes: Natural white light. *Nat. Photonics* **2010**, *4*, 738. [CrossRef]
15. El-Masry, N.A.; Piner, E.L.; Liu, S.X.; Bedair, S.M. Phase separation in InGaN grown by metalorganic chemical vapor deposition. *Appl. Phys. Lett.* **1998**, *72*, 40. [CrossRef]

16. Azadmand, M.; Barabani, L.; Bietti, S.; Chrastina, D.; Bonera, E.; Acciarri, M.; Fedorov, A.; Tsukamoto, S.; Nötzel, R.; Sanguinetti, S. Droplet controlled growth dynamics in molecular beam epitaxy of nitride semiconductors. *Sci. Rep.* **2018**, *8*, 11278. [CrossRef] [PubMed]
17. Lo, I.; Hsieh, C.H.; Hsu, Y.C.; Pang, W.Y.; Chou, M.C. Self-assembled GaN hexagonal micropyramid and microdisk. *Appl. Phys. Lett.* **2009**, *94*, 062105. [CrossRef]
18. Tsai, C.D.; Lo, I.; Wang, Y.C.; Yang, C.C.; You, S.T.; Yang, H.Y.; Huang, H.C.; Chou, M.M.C. Finite growth of InGaN/GaN triple-quantum-well microdisks on $LiAlO_2$ substrate. *AIP Adv.* **2018**, *8*, 095208. [CrossRef]